

Effect of a viscous fluid shell on the propagation of gravitational waves

Nigel T. Bishop Petrus J. van der Walt Monos Naidoo

Department of Mathematics, Rhodes University, Grahamstown, 6140, South Africa

Abstract

In this paper we show that there are circumstances in which the damping of gravitational waves (GWs) propagating through a viscous fluid can be highly significant; in particular, this applies to Core Collapse Supernovae (CCSNe). In previous work, we used linearized perturbations on a fixed background within the Bondi-Sachs formalism, to determine the effect of a dust shell on GW propagation. Here, we start with the (previously found) velocity field of the matter, and use it to determine the shear tensor of the fluid flow. Then, for a viscous fluid, the energy dissipated is calculated, leading to an equation for GW damping. It is found that the damping effect agrees with previous results when the wavelength λ is much smaller than the radius r_i of the matter shell; but if $\lambda \gg r_i$, then the damping effect is greatly increased.

Next, the paper discusses an astrophysical application, CCSNe. There are several different physical processes that generate GWs, and many models have been presented in the literature. The damping effect thus needs to be evaluated with each of the parameters λ, r_i and the coefficient of shear viscosity η , having a range of values. It is found that in most cases there will be significant damping, and in some cases that it is almost complete.

We also consider the effect of viscous damping on primordial gravitational waves (pGWs) generated during inflation in the early Universe. Two cases are investigated where the wavelength is either much shorter than the shell radii or much longer; we find that there are conditions that will produce significant damping, to the extent that the waves would not be detectable.

1 INTRODUCTION

We have shown, previously, that a dust shell surrounding a GW event modifies a gravitational (GW) wave in both magnitude and phase [1], and extended the

analysis to show that a burst of GWs can, in principle, lead to echoes [2], although, in practice, an astrophysical scenario that would produce a discernible echo is unlikely. We further showed that the results are astrophysically relevant: the GW signal from events including core collapse supernovae (CCSNe) and binary neutron star (BNS) mergers can be changed so that the modification is measurable [2]. A key point about these effects is that the magnitude is proportional to λ/r_i , where λ is the GW wavelength and r_i is the matter shell radius.

GWs travelling through a perfect fluid do not experience any absorption or dissipation [3] as noted in [4]. However, Hawking [5] showed that in the case of nonzero shear viscosity, η , GWs travelling through such a fluid would interact with the matter losing energy to the medium and energy dissipation would occur, with a damping rate proportional to $16\pi\eta$; see also [6, 7, 8].

In this paper, we calculate the effect of a viscous matter shell on GW propagation. The procedure is straightforward, but the intermediate algebraic expressions involve many terms, and so the calculation is handled using computer algebra. The starting point is a solution to the Einstein equations linearized about Minkowski in Bondi-Sachs form. The velocity field of dust in this spacetime is found, and from there it is a straightforward calculation to find the fluid shear tensor σ_{ab} , and thence the rate of energy dissipation due to viscosity. The result obtained reduces to previous results when $r_i \gg \lambda$, see Eq. (19). However, when $\lambda \gg r_i$ the damping effect can be large, see Eq. (21); to our knowledge, this case has not been considered previously.

We next apply Eq. (21) to the astrophysical case of CCSNe. CCSNe have long been regarded as a potential GW source for detection by LIGO/Virgo, but to date no such events have been observed. The modeling of CCSNe involves many aspects of matter physics; we review this literature, and so determine a value range for each parameter used in our model. The wavelength range is 300 to 3000 km, corresponding to 100 to 1000 Hz, and the source region radius range is 10 to 30 km so that Eq. (21) can be applied. There are reported values of the shear viscosity that lead to almost complete damping of the GW signal, whereas if the viscosity is somewhat lower then only the lower frequencies in the GW signal would be damped out.

As a further case study, we consider primordial gravitational waves (pGWs) generated during the epoch of cosmic inflation. Here, we set up an early Universe scenario where a discrete source generates pGWs, which are subsequently affected by viscous matter under the extreme conditions of the early Universe. Two cases are considered where the wavelength is either much shorter than the shell radii or alternatively much longer. In both cases there are conditions that will produce significant damping, to the extent that the waves will not be detectable.

In Section 2 we discuss perturbations about Minkowski spacetime in the Bondi-

Sachs formalism, and find the velocity field and then the shear tensor of the fluid flow. We then consider energy loss due to shear viscosity in Section 3. The consequences to astrophysics are considered, in general, in Section 4. We consider the effects of a viscous fluid shell on the propagation of GWs in CCSNe in Section 5, and in Section 6 we investigate the effects on pGWs. We summarise our results and conclusions in Section 7.

We use geometric units in this paper, with the gravitational constant G and the speed of light c set to unity. However, results from the astrophysical literature are reported in SI units, and then used with the appropriate conversion factors.

2 USING BONDI-SACHS FORMALISM

We use the formalism developed previously [1, 2] on GWs propagating through matter shells. The metric is in Bondi-Sachs form

$$ds^2 = - (e^{2\beta} (1 + rW_c) - r^2 h_{AB} U^A U^B) du^2 - 2e^{2\beta} dudr - 2r^2 h_{AB} U^B dudx^A + r^2 h_{AB} dx^A dx^B, \quad (1)$$

where $h^{AB} h_{BC} = \delta_C^A$, and the condition that r is a surface area coordinate implies $\det(h_{AB}) = \det(q_{AB})$ where q_{AB} is a unit sphere metric (e.g. $d\theta^2 + \sin^2 \theta d\phi^2$). We represent q_{AB} by a complex dyad (e.g. $q^A = (1, i/\sin\theta)$) and introduce the complex differential angular operators $\bar{\partial}, \partial$ [9], with the operators defined with respect to the unit sphere as detailed in [10, 11]. Then h_{AB} is represented by the complex quantity $J = q^A q^B h_{AB}/2$ (with $J = 0$ characterizing spherical symmetry), and we also introduce the complex quantity $U = U^A q_A$. We make the ansatz of a small perturbation about Minkowski spacetime with the metric quantities β, U, W, J taking the form

$$\begin{aligned} \beta &= \Re(\beta^{[2,2]}(r)e^{i\nu u})_0 Z_{2,2}, & U &= \Re(U^{[2,2]}(r)e^{i\nu u})_1 Z_{2,2}, & W_c &= \Re(W_c^{[2,2]}(r)e^{i\nu u})_0 Z_{2,2}, \\ J &= \Re(J^{[2,2]}(r)e^{i\nu u})_2 Z_{2,2}, \end{aligned} \quad (2)$$

The perturbations oscillate in time with frequency $\nu/(2\pi)$. The quantities ${}_s Z_{\ell,m}$ are spin-weighted spherical harmonic basis functions related to the usual ${}_s Y_{\ell,m}$ as specified in [12, 10]. They have the property that ${}_0 Z_{\ell,m}$ are real, enabling the description of the metric quantities β, W (which are real) without mode-mixing; however, for $s \neq 0$ ${}_s Z_{2,2}$ is, in general, complex. A general solution may be constructed by summing over the (ℓ, m) modes, but that is not needed here, since we are considering a source that is continuously emitting GWs at constant frequency dominated by the $\ell = 2$ (quadrupolar) components.

As shown in previous work [12, 1], solving the vacuum Einstein equations under the condition of no incoming radiation leads to

$$\begin{aligned}
\beta^{[2,2]} &= b_0, \\
W_c^{[2,2]} &= 4i\nu b_0 - 2\nu^4 C_{40} - 2\nu^2 C_{30} + \frac{4i\nu C_{30} - 2b_0 + 4i\nu^3 C_{40}}{r} + \frac{12\nu^2 C_{40}}{r^2} \\
&\quad - \frac{12i\nu C_{40}}{r^3} - \frac{6C_{40}}{r^4}, \\
U^{[2,2]} &= \frac{\sqrt{6}(-2i\nu b_0 + \nu^4 C_{40} + \nu^2 C_{30})}{3} + \frac{2\sqrt{6}b_0}{r} + \frac{2\sqrt{6}C_{30}}{r^2} - \frac{4i\nu\sqrt{6}C_{40}}{r^4} \\
&\quad - \frac{3\sqrt{6}C_{40}}{r^4}, \\
J^{[2,2]} &= \frac{2\sqrt{6}(2b_0 + i\nu^3 C_{40} + i\nu C_{30})}{3} + \frac{2\sqrt{6}C_{30}}{r} + \frac{2\sqrt{6}C_{40}}{r^3}, \tag{3}
\end{aligned}$$

with constants of integration b_0, C_{30}, C_{40} . The gravitational news \mathcal{N} is defined in a coordinate system that satisfies the Bondi gauge conditions $\lim_{r \rightarrow \infty} J, U, \beta, W/r = 0$, and is calculated on making the required coordinate transformation. The procedure in the general case was described in [13]. This was then simplified for the linearized approximation in [12] (Sec.3.3), with an explicit expression for the news given in [14], Eq. (16). Denoting the news for the solution Eq. (3) by \mathcal{N}_0 , and allowing for the conventions used here, we find $\mathcal{N}_0 = -\sqrt{6}\nu^3 \Re(iC_{40} \exp(i\nu u))_2 Z_{2,2}$. The rescaled gravitational wave strain and news are related (see Eq. (276) in [10]) $\mathcal{H}_0 = r(h_+ + ih_\times) = 2 \int \mathcal{N}_0 du$, giving

$$\mathcal{H}_0 = \Re(H_0 \exp(i\nu u))_2 Z_{2,2} \text{ with } H_0 = -2\sqrt{6}\nu^2 C_{40}. \tag{4}$$

Thus, C_{40} is determined by the physical problem being modelled, and b_0, C_{30} represent gauge freedoms.

We now suppose that the GWs pass through a shell of matter, and determine the velocity field V_a treating the matter as dust. The ansatz for V_a is similar to that for the metric, and is

$$\begin{aligned}
V_0 &= -1 + \Re(V_0^{[2,2]}(r)e^{i\nu u})_0 Z_{2,2}, \quad V_1 = -1 + \Re(V_1^{[2,2]}(r)e^{i\nu u})_0 Z_{2,2}, \\
q^A V_A &= \Re(V_{ang}^{[2,2]}(r)e^{i\nu u})_1 Z_{2,2}. \tag{5}
\end{aligned}$$

Then solving the matter conservation condition $\nabla_a(\rho v^a V^b) = 0$, which in this case

is equivalent to the geodesic condition, leads to

$$\begin{aligned}
V_0^{[2,2]}(r) &= \frac{1}{r^3} \times \\
&\quad (3C_{40} - 2ir^3\nu C_{30} - 2ir^3\nu^3 C_{40} + 6i\nu C_{40}r - 2i\nu b_0 r^4 + \nu^2 r^4 C_{30} + \nu^4 r^4 C_{40} - 6C_{40}\nu^2 r^2) \\
V_1^{[2,2]}(r) &= i \frac{9C_{40} + 12i\nu C_{40}r + 2i\nu b_0 r^4 - \nu^2 r^4 C_{30} - \nu^4 r^4 C_{40} - 6C_{40}\nu^2 r^2}{r^4\nu} \\
V_{ang}^{[2,2]}(r) &= -\frac{i\sqrt{6}}{r^3\nu} \times \\
&\quad (3C_{40} - 2ir^3\nu C_{30} - 2ir^3\nu^3 C_{40} + 6i\nu C_{40}r - 2i\nu b_0 r^4 + \nu^2 r^4 C_{30} + \nu^4 r^4 C_{40} - 6C_{40}\nu^2 r^2) .
\end{aligned} \tag{6}$$

The contribution of viscosity to the stress-energy tensor of a viscous fluid is (see [15], p.139)

$$T_{ab} = -2\eta\sigma_{ab} - \zeta\theta P_{ab}, \tag{7}$$

where η, ζ are the coefficients of shear and bulk viscosity; θ is the fluid expansion, σ_{ab} is the shear tensor, and P_{ab} is the projection tensor, given by

$$\begin{aligned}
\theta &= g^{ab}\nabla_a V_b, \quad P_{ab} = g_{ab} + V_a V_b, \\
\sigma_{ab} &= \frac{(P_{ac}\nabla_d V_b + P_{bc}\nabla_d V_a)g^{cd}}{2} - \frac{P_{ab}\theta}{3}.
\end{aligned} \tag{8}$$

The velocity field of Eq. (6) gives

$$\begin{aligned}
\theta &= \sigma_{00} = \sigma_{01} = \sigma_{0A} = 0, \\
-\sigma_{11}^{[2,2]} &= \sigma_W^{[2,2]} = 12C_{40} \frac{3i - 3r\nu - ir^2\nu^2}{r^5\nu} \\
\sigma_{1U}^{[2,2]} &= 2C_{40} \frac{6i - 6r\nu - 3ir^2\nu^2 + r^3\nu^3}{r^4\nu} \\
\sigma_J^{[2,2]} &= C_{40} \frac{-3 - 3ir\nu + 3r^2\nu^2 + 2ir^3\nu^3 - r^4\nu^4}{r^3\nu},
\end{aligned} \tag{9}$$

where the the above quantities are defined in terms of the usual separation of variables, i.e.,

$$\begin{aligned}
\sigma_{11} &= \Re(\sigma_{11}^{[2,2]}(r)e^{i\nu u})_0 Z_{2,2}, \quad q^A \sigma_{1A} = \Re(\sigma_{1U}^{[2,2]}(r)e^{i\nu u})_1 Z_{2,2}, \\
q^{AB} \sigma_{AB} &= \Re(\sigma_W^{[2,2]}(r)e^{i\nu u})_0 Z_{2,2}, \quad q^A q^B \sigma_{AB} = \Re(\sigma_J^{[2,2]}(r)e^{i\nu u})_2 Z_{2,2}.
\end{aligned} \tag{10}$$

It is interesting to note that the expressions in Eqs. (9) involve only the physical constant C_{40} , and not the gauge freedom constants b_0, C_{30} . Thus σ_{ab} is gauge independent.

3 ENERGY LOSS DUE TO VISCOSITY

We use the formula that the rate of energy loss per unit volume is $-2\eta\sigma_{ab}\sigma^{ab}$ where η is the coefficient of shear viscosity [15]. This quantity is evaluated using Eqs. (9), and then integrated over a shell of radius r and thickness δr ; the integration is straightforward because of the orthonormality of the angular basis functions ${}_s Z_{\ell,m}$. We find

$$\langle \dot{E}_\eta \rangle = -12\eta C_{40}^2 \nu^6 \delta r \left(1 + \frac{2}{r^2 \nu^2} + \frac{9}{r^4 \nu^4} + \frac{45}{r^6 \nu^6} + \frac{315}{r^8 \nu^8} \right), \quad (11)$$

where $\langle f \rangle$ denotes the average of $f(u)$ over a wave period, i.e.

$$\langle f \rangle = \frac{\nu}{2\pi} \int_0^{\frac{2\pi}{\nu}} f dt, \quad (12)$$

and where we have used $\langle \cos^2(\nu u) \rangle = \langle \sin^2(\nu u) \rangle = 1/2$ and $\langle \cos(\nu u) \sin(\nu u) \rangle = 0$. Now, the rate of energy being output in GWs is

$$\langle \dot{E}_{GW} \rangle = \frac{1}{4\pi} \oint |N|^2 = \frac{3C_{40}^2 \nu^6}{4\pi}, \quad (13)$$

so that

$$\langle \dot{E}_\eta \rangle = -16\pi\eta\delta r \langle \dot{E}_{GW} \rangle \left(1 + \frac{2}{r^2 \nu^2} + \frac{9}{r^4 \nu^4} + \frac{45}{r^6 \nu^6} + \frac{315}{r^8 \nu^8} \right). \quad (14)$$

Conservation of energy implies that the energy being absorbed by the viscous fluid must be balanced by a reduction in the GW energy. Thus

$$\langle \dot{E}_{GW} \rangle (r + \delta r) = \langle \dot{E}_{GW} \rangle (r) \left[1 - 16\pi\eta\delta r \left(1 + \frac{2}{r^2 \nu^2} + \frac{9}{r^4 \nu^4} + \frac{45}{r^6 \nu^6} + \frac{315}{r^8 \nu^8} \right) \right]. \quad (15)$$

As introduced earlier, H represents the magnitude of the GWs rescaled to allow for the $1/r$ fall-off, i.e. $H \propto r \langle |h_+, h_\times| \rangle$. Then $\langle \dot{E}_{GW} \rangle \propto H^2$ so that

$$H(r + \delta r) = H(r) \left[1 - 8\pi\eta\delta r \left(1 + \frac{2}{r^2 \nu^2} + \frac{9}{r^4 \nu^4} + \frac{45}{r^6 \nu^6} + \frac{315}{r^8 \nu^8} \right) \right]. \quad (16)$$

This leads to the differential equation

$$\frac{dH}{dr} = -8\pi\eta H \left(1 + \frac{2}{r^2 \nu^2} + \frac{9}{r^4 \nu^4} + \frac{45}{r^6 \nu^6} + \frac{315}{r^8 \nu^8} \right), \quad (17)$$

which is easily solved to give

$$H(r) = C \exp \left(-8\pi\eta \left(r - \frac{2}{r\nu^2} - \frac{3}{r^3\nu^4} - \frac{9}{r^5\nu^6} - \frac{45}{r^7\nu^8} \right) \right), \quad (18)$$

where C is a constant. There are two useful special cases. Let r_i, r_o be the inner and outer radii of the shell. If r_i, r_o are much larger than the wavelength λ of the GWs, then

$$H(r_o) = H(r_i) \exp(-8\pi\eta(r_o - r_i)). \quad (19)$$

Results equivalent to Eq. (19) have been given before, and some of the literature is reviewed in the Introduction, Section 1. If r_i is much smaller than the wavelength of the GWs with $r_o = \alpha r_i$ with $\alpha > 1$ then

$$H(r_o) = H(r_i) \exp \left(-\frac{360\pi\eta}{r_i^7\nu^8} (1 - \alpha^{-7}) \right) = H(r_i) \exp \left(-\frac{45\eta\lambda^8}{32r_i^7\pi^7} (1 - \alpha^{-7}) \right). \quad (20)$$

As $r_o \rightarrow \infty$, Eq.(20) reduces to

$$H(r_o) = H(r_i) \exp \left(-\frac{45\eta\lambda^8}{32r_i^7\pi^7} \right), \quad (21)$$

but the damping effect is reduced by only a little for a shell of finite thickness. For example, $(1 - \alpha^{-7})$ is 0.99 for $\alpha = 2$ and is 0.5 for $\alpha = 1.104$. To our knowledge, viscous damping of GWs with $r_i \ll \lambda$ has not been studied previously, and Eqs. (20) and (21) are new. In the next sections we investigate some astrophysical implications.

4 ASTROPHYSICAL APPLICATIONS: GENERAL CONSIDERATIONS

In the next section we will discuss core collapse supernovae (CCSNe), for which viscous damping of GWs can be significant. However, we first make some general comments. The model developed above uses a Minkowski background, rather than Schwarzschild or Kerr for CCSNe. Thus the numerical values that will be obtained should not be regarded as precise statements, but rather as estimates as to when the effect of viscous damping of GWs may be important.

A numerical relativity simulation of the full Einstein and matter field equations with GW extraction far from the source will properly include all effects described above. However, in situations such as CCSNe the complexity of the matter physics necessitates an approximate treatment of GW extraction, normally calculated using a modified quadrupole formula. These models do not consider viscous damping by matter outside the region where the GWs are generated.

Geometric units are used in this paper, but the astrophysical literature reports estimates of the shear viscosity in SI units ($\text{kg/m/s} = \text{Pa s}$), or sometimes in cgs units. The conversion requires multiplication by G/c^3 , where G is the gravitational constant and c is the speed of light; numerically, $G/c^3 = 2.477 \times 10^{-36} \text{s/kg}$.

5 CORE COLLAPSE SUPERNOVAE

CCSNe have been identified as candidates of sources of detectable GWs. Whilst binary black hole (BBH) and binary neutron star (BNS) mergers are currently the only GW events picked up by LIGO and VIRGO, supernovae are expected to produce, under certain conditions, GWs detectable by the current generation of interferometers or those on the horizon. For now, all detection of supernovae have been confined to electromagnetic detection. The GW signal from a supernova event would be different (but not altogether so) from the characteristic signal of a BBH merger or BNS merger.

Photons originate at the outer edge of a star and hence provide only limited information on the interior regions. The detection of GWs which are the result of the aspherical motion of the inner regions will provide a wealth of information on these regions and the mechanism leading to the supernova explosion, where all the four fundamental forces of nature are involved.

Whilst the central engines and inner regions of CCSNe have yet to be fully understood, there exist several studies of their progenitors and the subsequent evolution and detection [16, 17, 18]. For stars of mass larger than $8M_{\odot}$, evolution normally proceeds through several stages of core burning and then to core collapse once nuclear fusion halts when there are no further burning processes to balance the gravitational attraction. Typically, these cores are iron cores, with the critical mass signalling the onset of core collapse ranging from $1.3M_{\odot}$ to $1.7M_{\odot}$. The core breaks into two during the collapse, with the inner core of $0.4M_{\odot}$ to $0.6M_{\odot}$ in sonic contact and collapsing homologously and the outer core collapsing supersonically. The inner core reaches supranuclear densities of $\sim 2 \times 10^{14} \text{gm/cm}^3$ where the nuclear matter stiffens, resulting in a bounce of the inner core. The resulting shock wave is launched into the collapsing outer core. However, the shock loses energy to dissociation of iron nuclei, stalling at $\sim 150 \text{ km}$ within $\sim 10 \text{ ms}$ after formation. Many computationally demanding simulations exist [19, 20, 21] for generation of GWs from CCSNe.

The anticipated GW signal from CCSNe, is normally described by four phases. Initially there is the convection signal. This is followed by a quiescent phase. The third phase is driven by the standing-accretion-shock instability (SASI) and is also referred to as the neutrino convection phase. Finally, there is the explosion phase.

5.1 General-relativistic simulations of core-collapse supernovae

There has been a steady increase within the numerical relativity community of simulations of the evolution of CCSNe and we summarise some of the results of recent efforts giving some of the important parameter values.

Astrophysics with CCSNe GW signals in the next generation of GW detectors is discussed in [22] using the Supernova Model Evidence Extractor (SMEE) to capture the main features of GW signals from CCSNe using numerical relativity (NR) waveforms to create approximate models. These include features in the GW signal that are associated with g-modes and the standing accretion shock instability, and testing SMEE's performance using simulated data for planned future detectors, such as the Einstein Telescope, Cosmic Explorer, and LIGO Voyager. In third generation detector configurations, it was found that about 50% of neutrino-driven simulations were detectable at 100 kpc, and 10% at 275 kpc.

Scheidegger et al. [23] produced 25 gravitational waveforms from 3D magnetohydrodynamic (MHD) core-collapse simulations of a $15 M_{\odot}$ zero age main sequence star (ZAMS) progenitor star. They use a variety of rotation values from non-rotating to rapidly-rotating. Rotation leads to a large spike at core-bounce in the plus polarization only. The simulations are short duration as they were stopped up to 130 ms after the core bounce time.

Müller et al. [24] carried out 3D neutrino-driven CCSNe simulations of non-rotating stars. The waveforms have emission due to both SASI and g-modes. The GW signals extend to 1.3 s after core bounce, with the strongest GW emission in the first 0.7 s after the core bounce time. The Müller et al. waveforms do have g-mode emission, however it is relatively slow to develop and rarely approaches 300 Hz [24]. Simulations were performed with the general relativistic neutrino hydrodynamics code Vertex-CoCoNuT [25].

Andresen et al. [19] also carried out 3D neutrino-driven CCSN simulations of non-rotating stars. They find that the gravitational wave emission is dominated by late-time, long-lived convection in the proto-neutron star (PNS). This means that the GW energy produced stems mainly from the fluid dynamics within the PNS, and not from perturbations of the PNS by fluid dynamics above it. Their investigations were confined to rough estimates based on the expected excess power in second- and third generation GW detectors in two bands at low (20...250 Hz) and high (250...1200 Hz) frequency. Third-generation instruments like the Einstein Telescope, however, are expected to detect all of their models at the typical distance of a Galactic supernova (≈ 10 kpc) and strong GW emitters out to 50 kpc. The GWs were generated within a radius of 10^4 m to 2.8×10^4 m and if we were to consider this the boundary of the inner radius of our matter shell, then we

can take $10^4 \text{ m} \lesssim r_i \lesssim 2.8 \times 10^4 \text{ m}$.

Kuroda et al. [26] produced 3D simulations of a $15 M_\odot$ ZAMS progenitor star using three different equations of state (EOS) and a quadrupole approximation. For the SASI-origin emission, the peak value of GW energy spectrum appears at 129 Hz and reaches almost a comparable amplitude to that from g-mode oscillation. It is expected that GWs from Galactic SNe are likely observable even if their progenitors are non-rotating. For the SASI-origin emission, $r_i \approx 10^4 \text{ m}$, whilst from the other two models we have $10^4 \text{ m} \lesssim r_i \lesssim 2 \times 10^4 \text{ m}$.

Yakunin et al. [27] carried out one general relativistic, multi-physics, 3D simulation of a $15 M_\odot$ ZAMS progenitor star with state of the art weak interactions. They also find that the GW energy produced stems largely from the fluid dynamics within the PNS. However, in their model, the dominant emission stems from the convective region itself, rather than from the convective overshoot layer above it as in [19]. Their simulation is stopped 450 ms after core bounce. The strong GW emission starts at $\sim 120 \text{ ms}$ after core bounce when the SASI develops and the emission peaks at a higher frequency of 1000 Hz due to g-mode oscillations of the PNS surface. Again, $10^4 \text{ m} \lesssim r_i \lesssim 2 \times 10^4 \text{ m}$.

Powell et al. [28] generated two neutrino-driven simulations in 3D down to the innermost 10 km to include the PNS convection zone in spherical symmetry. The first simulation is the explosion of an ultra-stripped star in a binary system simulated from a star with an initial helium mass of $3.5 M_\odot$. The ultra-stripped simulation ends at 0.7 s after core bounce. The second is a single star with a ZAMS mass of $18 M_\odot$, which was simulated up to 0.9 s after core bounce. Both models have peak GW emission between 800 Hz and 1000 Hz due to g-mode oscillations of the PNS surface and both models have $r_i \approx 10^4 \text{ m}$.

Shibagaki et al. [29] considered GW and neutrino signals from full general relativistic 3-D hydrodynamics simulations of non-rotating and rapidly rotating stellar core-collapse. They find that the GW and neutrino signals would be simultaneously detectable by the current generation detectors up to $\approx 10 \text{ kpc}$. Their findings indicate that the joint observation of GWs and neutrinos is indispensable for extracting information on the PNS evolution preceding black hole formation. In the non-rotating case, $\Omega_0 = 0 \text{ rad s}^{-1}$, the GWs are generated within a radius of 10^4 m with a frequency of 200-300 Hz. In the $\Omega_0 = 1 \text{ rad s}^{-1}$ case, $r_i \sim 10^4 \text{ m}$, and the frequency of GWs are between 300-400 Hz. The $\Omega_0 = 2 \text{ rad s}^{-1}$ model produces GWs within a frequency range of 400-800 Hz also within a 10 km core.

A summary of the results is given in Table 1.

5.2 The viscosity for a shell surrounding a CCSNe

The viscosity in the core collapse environment has received only a little attention in the literature. Potential mechanisms for viscosity have been explored in [30],

Reference	r_i [m]	Frequency [Hz]
Roma [22]		96 - 1000
Scheidegger [23]		317 - 935
Müller [24]		130 - 1100
Andresen [19]	$10^4 - 2.8 \times 10^4$	100 - 700
Kuroda [26]	$10^4 - 2 \times 10^4$	100 - 671
Yakunin [27]	$10^4 - 2 \times 10^4$	200 - 600
Powell [28]	10^4	800 - 1000
Shibagaki [29]	10^4	200 - 800

Table 1: Parameter values from various references

and include neutrino viscosity, turbulent viscosity caused by the magnetorotational instability (MRI), and turbulent viscosity by entropy and composition-gradient-driven convection. The MRI was found to be the most effective dominating the neutrino viscosity by 2 to 3 orders of magnitude. Within the PNS, the authors [30] find that the MRI will operate and dominate the viscosity even for the slowest rotators considered.

Fig. 5 (left) of [30] plots values of the kinematic viscosity coefficient due the MRI against radius. In the region of the shell, say between 10 and 30 km, it varies in the range 10^{12} to 10^{14} cm^2s^{-1} . Multiplication by the density, about 10^{12} gm/cm^3 , gives the dynamic viscosity at 10^{23} to 10^{25} $\text{kg}/\text{m}/\text{s}$. Ref. [31] found values consistent with these magnitudes. Values for η in neutron star material are discussed in [32] (e.g., see Fig. 25), and can be as high as 10^{22} $\text{kg}/\text{m}/\text{s}$.

5.3 The damping effect on GWs emanating from CCSNe

Putting together the results from the previous two subsections, we consider the scenario of a CCSNe with GW emission in the frequency range 100 to 1000 Hz, the inner radius r_i of the matter surrounding the GW source in the range 10^4 to 3×10^4 m, and fluid viscosity η with a maximum value of 10^{25} $\text{kg}/\text{m}/\text{s}$. Since r_i is much smaller than the wavelength of the GWs, we can use Eq. (21). Fig. 1 plots the inner radius of the shell (r_i) on the x-axis (in m), the GW frequency (f) on the y-axis (in Hz), and $\log_{10}(\eta)$ on the z-axis, with η in $\text{kg}/\text{m}/\text{s}$. The surface plotted has damping factor 0.5, i.e. $H(r_o)/H(r_i) = 0.5$. Values of η a little above the surface would lead to (almost) complete damping, and those a little below would lead to (almost) no damping.

The figure shows that, except in the case that both f and r_i are towards the top of their ranges, GW viscous damping is expected to be significant.

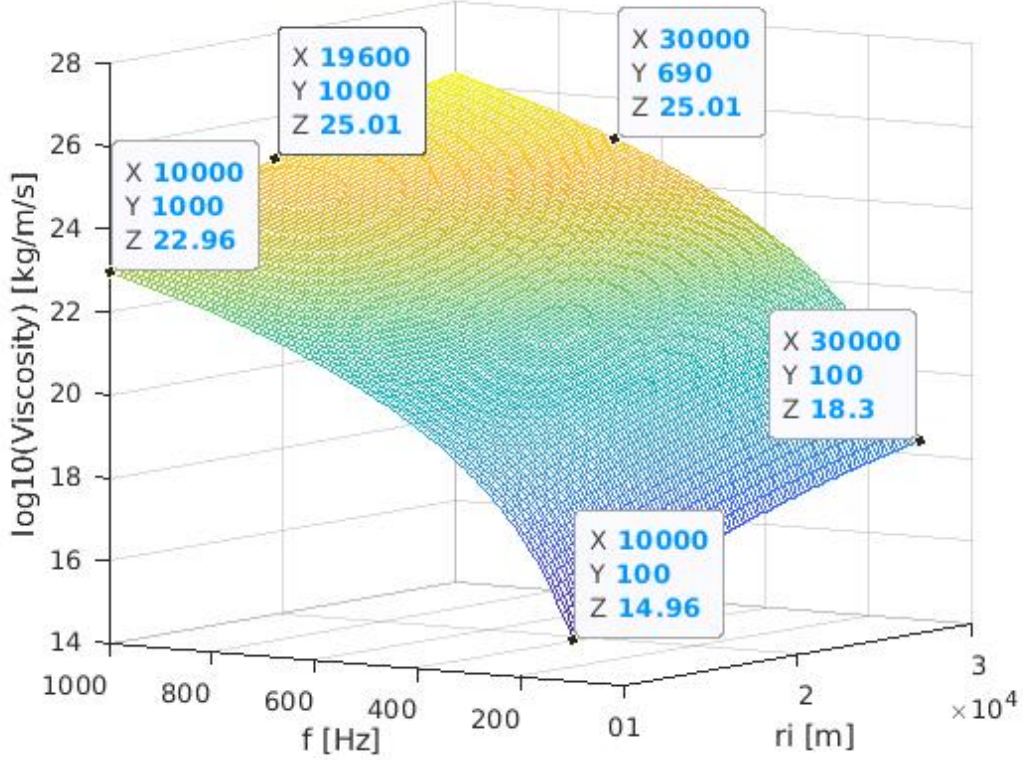


Figure 1: The figure plots the inner radius of the shell (r_i) on the x-axis (in m), the GW frequency (f) on the y-axis (in Hz), and $\log_{10}(\eta)$ on the z-axis, with η in kg/m/s. The surface plotted has damping factor 0.5, i.e. $H(r_o)/H(r_i) = 0.5$. Some points on the surface are labelled with their coordinate values, indicating which parts of the surface have $\eta > 10^{25}$ kg/m/s..

5.4 Detection of GWs from CCSNe

The frequency range of CCSNe and the sensitivity of various detectors is illustrated in Fig. 2. The expected frequency range of GWs from CCSNe lie between 10^2 and 10^3 Hz, corresponding to a wavelength range of between 3×10^6 and 3×10^5 m. The expected GW magnitude from CCSNe fell outside the sensitivity of LIGO. However, the range fell within the sensitivity of Advanced Ligo, on its first observation run aLIGO (O1). No GWs ascribed to CCSNe were detected on this run or on the subsequent runs, O2 and O3. As the sensitivity improves with each run, towards full design sensitivity, it is hopeful that the increased cachement region leads to the first detection of GWs from CCSNe.

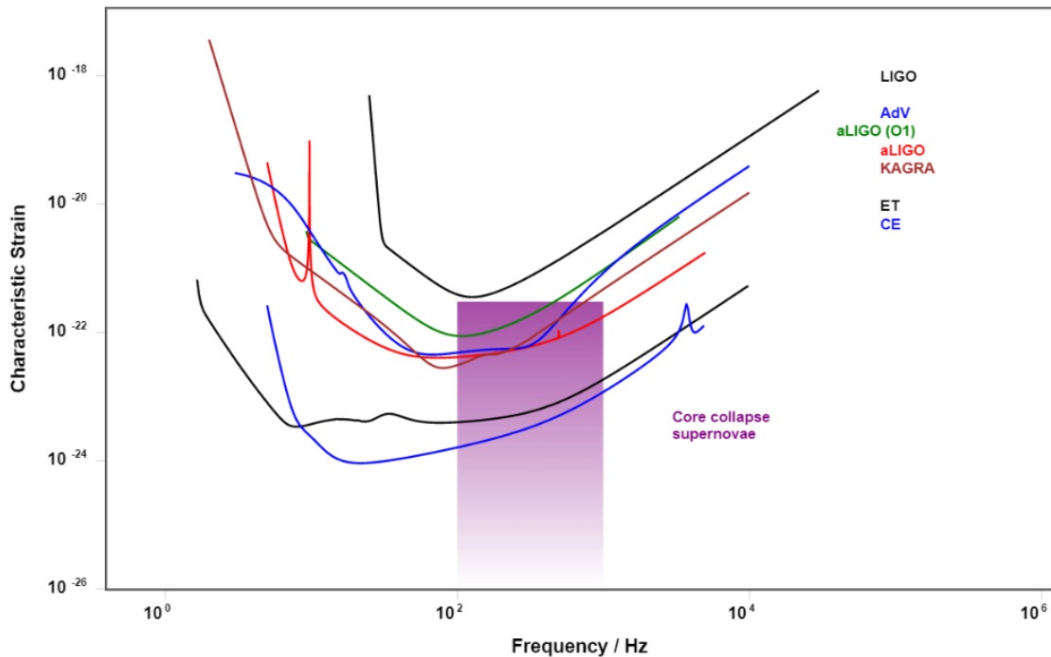


Figure 2: The signal range for CCSNe and sensitivities for various gravitational wave detectors, past, current and future for a source at 300kpc. Figure produced using the web-server reported in [33].

6 Primordial GWs

6.1 Background

In our previous work [1], we showed that the thin dust shell approximation can be extended to a thick shell by integrating over multiple shells and from this, we can model the dust-only effect on GWs in cosmology. Due to the extremely low density of the matter dominated Universe, the effect from astrophysical events was, however, found to be negligible. We now consider early Universe epochs where extreme temperatures and density conditions are expected. Primordial gravitational waves (pGWs) are of considerable interest in these epochs since direct observations from electromagnetic radiation are limited to the region after the surface of last scattering, around 370,000 years after the Big Bang, and the expected low interaction of GWs with matter then provides information from very early times. With detection and interpretation of these waves, theories of the early Universe, such as inflation, can then become accessible to direct observation. Similarly, theories of high-energy physics, that go beyond Earth-bound accelerators can also be tested, e.g., probing

matter properties in extreme temperatures. Interpreting pGW signals from their interaction with their environment is therefore highly important.

In early works, such as that of Hawking in 1966 [34], it was already shown that shear viscosity, η , will affect pGWs through damping. These results along with the work of Eckart in the 1940s [35] were consolidated and further developed into what can be considered the seminal work on primordial dissipative processes by Weinberg in 1971 [36]. Since then, there has been significant progress in understanding the details of early epochs and their physical properties but the work of Weinberg is still relevant as baseline formulae for relativistic viscous effects. Accordingly, we will setup representative early Universe scenarios to illustrate the viscous shell effects on pGW in the extreme conditions expected in the epoch after cosmic inflation ends. While recognising that pGWs generated during inflation are expected to be fundamentally stochastic (see [37]), for our purposes here, we will consider a discrete source of pGWs and reserve extending our work to better model the stochastic nature of pGWs for future research.

6.2 Cosmological scenario

In order to illustrate the possible effects of viscosity in cosmology, we consider an early Universe scenario based on quantities derived from the standard model and some classical references. We make use of the Friedman-Lemaître-Robertson-Walker (FLRW) geometry for a homogeneous and isotropic universe with the metric as

$$ds^2 = -dt^2 + a^2(t)\gamma_{ij}dx^i dx^j, \quad (22)$$

with γ_{ij} being the 3-space metric of maximal symmetry and $a(t)$ the scale factor.

Based on the present time as $t = 13.7\text{Gyr}$ ($= 4.32 \times 10^{18}\text{s}$) with $T = 2.725\text{K}$, we normalise the scale factor to be $a_0 = 1$ at present. Evolving back in time, the density of radiation and matter were approximately equal at $t = 56,000\text{yr}$ ($1.7662 \times 10^{12}\text{s}$) and $T = 9,000\text{K}$. Prior to that time but after inflation, the Universe can be treated as a radiation dominated Einstein de Sitter model with $a(t) \propto t^{1/2}$. During inflation the expansion is exponential with $a(t) \propto \exp(\mathbf{H}t)$ where \mathbf{H} is the Hubble constant – we use this notation to avoid confusion with the rescaled GW strain H .

At the end of inflation at $t = 10^{-32}\text{s}$ and $T = 10^{27}$ to 10^{28}K . According to [38] (Section 28.1), T is proportional to $1/a(t)$. Thus, at the end of inflation, we take $a = 10^{-27}$. The inverse of the Hubble rate does not change during inflation and is taken as $1/\mathbf{H}(= a/\dot{a}) = 10^{-35}\text{s}$, which leads to the horizon scale as $c/\mathbf{H} = 3 \times 10^{-27}\text{m}$.

Current ground-based GW detectors operate, approximately, in the frequency range 10 to 10^3Hz ; pulsar timing arrays and the planned satellite system LISA

will extend the lower limit to about 10^{-9} Hz. Thus searches for pGWs will cover wavelengths in the range 3×10^5 m to 3×10^{17} m. Since wavelength scales as $a(t)$, this corresponds to a wavelength range at the end of inflation of 3×10^{-22} to 3×10^{-10} m.

From Weinberg 1971 [36], rewritten with $c \neq 1$, we get

$$\tau = \left(\frac{16\pi G\eta}{c^2} \right)^{-1}, \quad (23)$$

for graviton interaction, where τ is the particle mean free time and further

$$\eta = \frac{4}{15} a T^4 \tau / c, \quad (24)$$

again rewritten with $c \neq 1$. Then eliminating τ from the two equations, we get

$$\eta^2 = \frac{a T^4 c}{60\pi G}. \quad (25)$$

When $T = 10^{27}$ K,

$$\eta = 3.68 \times 10^{58} \text{ kg/m/s} \quad (26)$$

This value of η is very large, and even when multiplied by G/c^3 to convert to geometric units, we get a value of $9.09 \times 10^{22} \text{m}^{-1}$.

If we consider a thin shell scenario where r_i, r_o are much larger than the wavelength λ , using Eq. (19) with $r\nu \gg 1$ and rewriting in terms of t , we have

$$\frac{dH}{dr} = -8\pi\eta H \rightarrow \frac{dH}{dt} = -8\pi\eta c H.$$

Now, η behaves as T^2 , i.e. as $1/a^2$ and further, we are in the radiation dominated era and a behaves as $t^{1/2}$. Thus η behaves as $1/t$ and we have $dH/dt = -8\pi\eta_i c H t_i/t$ with $\eta_i = 9.09 \times 10^{22}$ and $t_i = 10^{-32}$. Let $A = 8\pi\eta_i c t_i = 6.9$, then integrating

$$\frac{dH}{H} = -A \frac{dt}{t} \quad (27)$$

we get

$$H_o = H_i \left(\frac{t_i}{t_o} \right)^A. \quad (28)$$

For example, suppose that

$$t_o = 2t_i \text{ then } H_o = 0.009 H_i. \quad (29)$$

Although it is believed that after inflation the universe entered a quark-gluon phase and so behaved as an almost ideal fluid, this example shows that if η is as large as the value in Eq. (26) then the damping effect is so rapid that it may occur before the quark-gluon phase is reached.

Otherwise, considering that the wavelength is in the range of 3×10^{-22} to 3×10^{-10} m while the horizon scale is $c/H = 3 \times 10^{-27}$ m, the case for $r_i, r_o \ll \lambda$ can be justified and Eq. (21) becomes applicable. Using the same formulation, significant damping can then occur for even small values of η . As opposed to the first scenario where the value of η dominates damping, this effect is present in geometries where the (λ/r_i) ratio is large, which amplifies the value of the negative exponent in Eq. (21).

As an example, suppose that $r_i = 3 \times 10^{-27}$ m (a pGW source the size of the horizon scale) with $\lambda = 3 \times 10^{-22}$ m (the lower wavelength limit), then $H_o = 0.5H_i$ for $\eta = 2.0 \times 10^{25}$ kg/m/s. This value is much smaller than that of Eq. (26), and is of the same order as values considered for CCSNe. The timescale of the damping is 10^{-35} s, which is much shorter than the timescale of inflation.

7 SUMMARY AND CONCLUSIONS

We have investigated, using the Bondi-Sachs form of the Einstein equations linearized about Minkowski, the effect of viscosity on GW propagation. A general expression for the damping effect, Eq. (18), was found, which reduces to a known result, Eq. (19), in the case $\lambda \ll r_i$. However, when $\lambda \gg r_i$, Eq. (21) applies, which is a novel result. In this case, viscous damping of GWs can be astrophysically important since the effect includes the factor $[\lambda/(\pi r_i)]^7$ which can be large.

The paper then looked at the astrophysical application of CCSNe, but first noting that the model obtained may not be directly applicable so the results should be regarded as estimates rather than as precise predictions.

A number of CCSNe models have been proposed, and it was found that in many cases significant viscous damping of GWs was predicted. GW generation in CCSNe involves a number of different physical processes, each with GW output at a different frequency. It may be that a GW observation of a CCSNe event would see only the higher frequencies, with the lower ones completely damped out; such an observation could be used to constrain a combination of η and r_i .

We further considered pGWs generated in the early Universe during inflation where the viscous shell model can be applicable. As illustration, a high viscosity configuration was evaluated where $r_i, r_o \gg \lambda$, which resulted in significant damping. A further example considered, was the case $r_i \ll \lambda$. In this scenario, complete damping is predicted for even low viscosity values when the (λ/r_i) ratio is high. While these are rather speculative scenarios, we have illustrated that significant

pGW damping is possible within reasonable parameter ranges when the combination of geometry and physics allow for viscous shell modelling. On the other hand, if pGWs are detected, the results obtained here would constrain certain physical parameters of the early Universe: the value of the viscosity η would need to be significantly lower than that in Eq. (26); and there would be a wavelength-dependent constraint on a function of r_i and η .

Conflict of interest

The authors declare that they have no conflict of interest.

A Computer algebra scripts

The computer algebra scripts used in this paper are written in Maple in plain text format, and are available as Supplementary Material. The output file may be viewed using a plain text editor with line-wrapping switched off.

The file driving the calculation is `ViscousShell.map`, and it takes input from the files `gamma.out`, `initialize.map`, `lin.map` and `ProcRules.map`; the output is in `ViscousShell.out`. The Maple script is adapted from that reported in our previous work [1]. It first calculates and outputs the metric coefficients given in Eqs. (3), and it then substitutes this solution into the Einstein equations and checks that they are all satisfied. The next step is to use the matter conservation conditions for dust, obtaining Eqs. (6) for the fluid velocity field; the script also checks that the solution obtained satisfies the geodesic conditions. Next, the shear tensor σ_{ab} and the expansion θ are found, giving Eqs. (9). Next, we evaluate the expression $-2\eta\sigma_{ab}\sigma^{ab}$, integrate the result over a spherical shell of radius r and thickness δr , and find the time average; the result is Eq. (11).

References

- [1] N.T. Bishop, P.J. van der Walt, M. Naidoo, Effect of a low density dust shell on the propagation of gravitational waves, *Gen. Rel. Grav.* **52**(9), 92 (2020). DOI 10.1007/s10714-020-02740-9
- [2] M. Naidoo, N.T. Bishop, P.J. van der Walt, Modifications to the signal from a gravitational wave event due to a surrounding shell of matter, *Gen. Rel. Grav.* **53**(8), 77 (2021). DOI 10.1007/s10714-021-02841-z

- [3] J. Ehlers, A.R. Prasanna, R.A. Breuer, Propagation of Gravitational Waves Through Pressureless Matter, *Class. Quant. Grav.* **4**, 253 (1987). DOI 10.1088/0264-9381/4/2/009
- [4] B.Q. Lu, D. Huang, Y.L. Wu, Y.F. Zhou. Damping of gravitational waves in a viscous Universe and its implication for dark matter self-interactions (2018)
- [5] S.W. Hawking, Perturbations of an expanding universe, *Astrophys. J.* **145**, 544 (1966). DOI 10.1086/148793
- [6] J. Madore, The absorption of gravitational radiation by a dissipative fluid, *Commun. Math. Phys.* **30**, 335 (1973). DOI 10.1007/BF01645508
- [7] A.R. Prasanna, Propagation of gravitational waves through a dispersive medium, *Phys. Lett. A* **257**, 120 (1999). DOI 10.1016/S0375-9601(99)00313-8
- [8] G. Goswami, G.K. Chakravarty, S. Mohanty, A. Prasanna, Constraints on cosmological viscosity and self-interacting dark matter from gravitational wave observations, *Physical Review D* **95**, 103509 (2017). DOI 10.1103/PhysRevD.95.103509
- [9] E.T. Newman, R. Penrose, Note on the Bondi-Metzner-Sachs group, *J. Math. Phys.* **7**(5), 863 (1966). DOI 10.1063/1.1931221
- [10] N.T. Bishop, L. Rezzolla, Extraction of gravitational waves in numerical relativity, *Living Rev. Relativ.* **19**, 1 (2016). DOI DOI10.1007/s41114-016-0001-9. URL <http://dx.doi.org/10.1007/s41114-016-0001-9>
- [11] R. Gómez, L. Lehner, P. Papadopoulos, J. Winicour, The eth formalism in numerical relativity, *Class. Quantum Grav.* **14**(4), 977 (1997)
- [12] N.T. Bishop, Linearized solutions of the Einstein equations within a Bondi-Sachs framework, and implications for boundary conditions in numerical simulations, *Class. Quantum Grav.* **22**(12), 2393 (2005). DOI 10.1088/0264-9381/22/12/006
- [13] N.T. Bishop, R. Gómez, L. Lehner, M. Maharaj, J. Winicour, High-powered gravitational news, *Phys. Rev. D* **56**, 6298 (1997). DOI 10.1103/PhysRevD.56.6298
- [14] C. Reisswig, N.T. Bishop, C.W. Lai, J. Thornburg, B. Szilagyi, Characteristic evolutions in numerical relativity using six angular patches, *Classical and Quantum Gravity* **24**, 327 (2007). DOI 10.1088/0264-9381/24/12/S21

- [15] T.W. Baumgarte, S.L. Shapiro, Numerical Relativity: Solving Einstein's Equations on the Computer (Cambridge University Press, Cambridge, UK, 2010)
- [16] B. Müller, Hydrodynamics of core-collapse supernovae and their progenitors, *Astrophysics* **6**, 3 (2020). DOI 10.1007/s41115-020-0008-5
- [17] E. Abdikamalov, G. Pagliaroli, D. Radice. *Gravitational Waves from Core-Collapse Supernovae* (2020)
- [18] S.E. Woosley, A. Heger, T.A. Weaver, The evolution and explosion of massive stars, *Rev. Mod. Phys.* **74**, 1015 (2002)
- [19] H. Andresen, B. Müller, E. Müller, H.T. Janka, Gravitational Wave Signals from 3D Neutrino Hydrodynamics Simulations of Core-Collapse Supernovae, *Mon. Not. Roy. Astron. Soc.* **468**(2), 2032 (2017). DOI 10.1093/mnras/stx618
- [20] H. Andresen, E. Müller, H. Janka, A. Summa, K. Gill, M. Zanolin, Gravitational waves from 3D core-collapse supernova models: The impact of moderate progenitor rotation, *Mon. Not. Roy. Astron. Soc.* **486**(2), 2238 (2019). DOI 10.1093/mnras/stz990
- [21] D. Radice, V. Morozova, A. Burrows, D. Vartanyan, H. Nagakura, Characterizing the Gravitational Wave Signal from Core-Collapse Supernovae, *Astrophys. J. Lett.* **876**(1), L9 (2019). DOI 10.3847/2041-8213/ab191a
- [22] V. Roma, J. Powell, I.S. Heng, R. Frey, Astrophysics with core-collapse supernova gravitational wave signals in the next generation of gravitational wave detectors, *Phys. Rev. D* **99**(6), 063018 (2019). DOI 10.1103/PhysRevD.99.063018
- [23] S. Scheidegger, R. Kaeppli, S.C. Whitehouse, T. Fischer, M. Liebendoerfer, The Influence of Model Parameters on the Prediction of Gravitational wave Signals from Stellar Core Collapse, *Astron. Astrophys.* **514**, A51 (2010). DOI 10.1051/0004-6361/200913220
- [24] E. Muller, H.T. Janka, A. Wongwathanarat, Parametrized 3D models of neutrino-driven supernova explosions: Neutrino emission asymmetries and gravitational-wave signals, *Astron. Astrophys.* **537**, A63 (2012). DOI 10.1051/0004-6361/201117611
- [25] B. Müller, H.T. Janka, H. Dimmelmeier, A New Multi-dimensional General Relativistic Neutrino Hydrodynamic Code for Core-collapse Supernovae. I. Method and Code Tests in Spherical Symmetry, *Astrophys. J. Suppl. Ser.* **189**, 104 (2010). DOI 10.1088/0067-0049/189/1/104

- [26] T. Kuroda, K. Kotake, T. Takiwaki, A new Gravitational-wave Signature From Standing Accretion Shock Instability in Supernovae, *Astrophys. J. Lett.* **829**(1), L14 (2016). DOI 10.3847/2041-8205/829/1/L14
- [27] K.N. Yakunin, A. Mezzacappa, P. Marronetti, E.J. Lentz, S.W. Bruenn, W.R. Hix, O.E. Bronson Messer, E. Endeve, J.M. Blondin, J.A. Harris. The Gravitational Wave Signal of a Core Collapse Supernova Explosion of a 15 M_{\odot} Star (2017)
- [28] J. Powell, B. Müller, Gravitational Wave Emission from 3D Explosion Models of Core-Collapse Supernovae with Low and Normal Explosion Energies, *Mon. Not. Roy. Astron. Soc.* **487**(1), 1178 (2019). DOI 10.1093/mnras/stz1304
- [29] S. Shibagaki, T. Kuroda, K. Kotake, T. Takiwaki, Characteristic Time Variability of Gravitational-Wave and Neutrino Signals from Three-dimensional Simulations of Non-Rotating and Rapidly Rotating Stellar Core-Collapse, *Mon. Not. Roy. Astron. Soc.* **502**(2), 3066 (2021). DOI 10.1093/mnras/stab228
- [30] T.A. Thompson, E. Quataert, A. Burrows, Viscosity and Rotation in Core-Collapse Supernovae, *Astrophys. J.* **620**, 861 (2005). DOI 10.1086/427177
- [31] H.C. Spruit, Dynamo action by differential rotation in a stably stratified stellar interior, *Astron. Astrophys.* **381**, 923 (2002). DOI 10.1051/0004-6361:20011465
- [32] E.E. Kolomeitsev, D.N. Voskresensky, Viscosity of neutron star matter and r -modes in rotating pulsars, *Phys. Rev. C* **91**(2), 025805 (2015). DOI 10.1103/PhysRevC.91.025805
- [33] C.J. Moore, R.H. Cole, C.P.L. Berry, Gravitational-wave sensitivity curves, *Class. Quant. Grav.* **32**(1), 015014 (2015). DOI 10.1088/0264-9381/32/1/015014
- [34] S.W. Hawking, Perturbations of an Expanding Universe, *The Astrophysical Journal* **145**, 544 (1966). DOI 10.1086/148793
- [35] C. Eckart, The thermodynamics of irreversible processes. III. relativistic theory of the simple fluid, *Phys. Rev.* **58**(10), 919 (1940)
- [36] S. Weinberg, Entropy generation and the survival of protogalaxies in an expanding universe, *The Astrophysical Journal* **168**, 175 (1971). DOI 10.1086/151073

- [37] C. Caprini, D.G. Figueroa, Cosmological backgrounds of gravitational waves, *Classical and Quantum Gravity* **35**, 163001 (2018). DOI 10.1088/1361-6382/aac608
- [38] C.W. Misner, etc., K.S. Thorne, J.A. Wheeler, Gravitation (W.H. Freeman, New York, NY, 1973)